Synergistic latency reversal by the IAP antagonist AZD5582 and BET inhibitor JQ1, combined with Nef ablation, facilitates immune-mediated elimination of latently HIV-1-infected T-cells

Dylan Postmus[1,2], Sui Ting Hui[2], Bengisu Akbil[1], Jenny Jansen[1], Dominic Wooding[1], Oya Cingöz[1,3], Christine Goffinet[1,2]

[1]Institute of Virology, Charité - Universitätsmedizin Berlin, Corporate Member of Freie Universität Berlin and Humboldt-Universität zu Berlin, Berlin, Germany

[2]Department of Tropical Disease Biology, Liverpool School of Tropical Medicine, Pembroke Place, Liverpool L3 5QA, U.K.

[3]Medical Research Council (MRC) - University of Glasgow, Centre for Virus Research (CVR), Glasgow, U.K.

Christine Goffinet, Liverpool School of Tropical Medicine, Pembroke Place Liverpool, L3 5QA Liverpool, U.K.

Phone: +44(0)151 705 3100

e-mail: christine.goffinet@lstmed.ac.uk

ABSTRACT

The 'shock-and-kill' strategy can reactivate latent HIV-1 *in vivo* but has failed to meaningfully reduce the reactivatable reservoir, suggesting insufficient immunological visibility of infected cells. To investigate latency reversal agent (LRA)-specific shortcomings, we developed a novel HIV-1 latency model - Jurkat E6.1 subclonal T-cell lines, each harbouring a single, full-length, NL4.3-based provirus with a GFP_{OPT} reporter in the Env V5 loop - and quantified HIV-1 reactivation, Env surface presentation across LRAs and synergistically acting combinations. Bryostatin-1 induced GBP5-mediated restriction of surface Env and resistance to apoptosis. Bryostatin-1/JQ1 synergised for HIV-1 reactivation and boosted levels of cell-surface Env, but failed to reduce resistance to apoptosis. AZD5582/JQ1 boosted cell-surface Env levels, without co-induction of GBP5, T-cell activation or apoptotic resistance. HIV-1 Nef antagonised cytotoxic killing of HIV-1-reactivating T-cells - its knockout, combined with AZD5582/JQ1, achieved the highest immune-mediated elimination of latently infected T-cells, representing a promising HIV cure approach.

Keywords

HIV-1; HIV cure; 'shock-and-kill'; latency reversal; LRA; bryostatin-1; JQ1; AZD5582; ADCC; apoptosis; Env

INTRODUCTION

Recent rollbacks in international aid funding threaten the progress made globally in controlling and curbing the HIV pandemic, with the resulting disruptions in supply chains for antiretroviral therapy (ART) predicted to result in up to 10.75 million new infections in low- and middle-income countries between 2025 and 2030[1]. More than ever, these developments underscore the pressing need to establish an accessible, scalable and affordable cure strategy for people living with HIV (PLWH).

47 To this end, the 'shock-and-kill' cure strategy proposes the transcriptional reactivation of
48 the latent provirus, with the aim of rendering infected cells immunologically visible, a key
49 requirement for cytotoxic killing by patrolling immune cells. While conceptually promising, several
50 in-human clinical trials attempting this intervention have fallen short of the desired outcome.
51 Notably, the ROADMAP[2] and eCLEAR[3] trials, both of which administered the histone deacetylase
52 inhibitor (HDACi) romidepsin, in combination with the broadly neutralising, CD4 binding site-
53 targeting, anti-HIV-1 Envelope (Env) antibody 3BNC117, showed varying efficacies in delaying
54 viral rebound post-treatment interruption. The ROADMAP trial demonstrated significant but
55 modest increases in cell-associated unspliced HIV RNA (1.14 median fold increase) and
56 detectable viral RNA copies in serum for the romidepsin/3BNC117 combination-treated group.
57 The eCLEAR trial, which administered this intervention in newly diagnosed PLWH shortly after
58 ART initiation, failed to report a statistically significantly enhanced reduction of the size of the viral
59 reservoir as compared to the decay detected after treatment with ART alone. Additional
60 knowledge on 'shock-and-kill' approaches has been generated in animal models of HIV-1
61 infection, such as HIV-1-infected humanised mice and SIV-infected non-human primates (NHPs),
62 using LRAs of different classes such as inhibitors of inhibitor of apoptosis proteins (iIAPs)[4] and
63 inhibitors of bromodomain and extraterminal motif proteins (iBETs)[5]. Importantly, a landmark
64 study in NHPs identified the combination of the iIAP AZD5582 with SIV-specific anti-Env
65 antibodies was able to reduce, significantly, the number of intact proviruses in lymph nodes, but
66 not the peripheral blood or spleens of ART-treated rhesus macaques[6]. While this approach
67 showed promise, it did not achieve functional cure. Collectively, the continuous inability of 'shock-
68 and-kill' attempts *in vivo* to achieve cure likely reflects our lack of detailed understanding of the
69 pro- and antiviral impacts individual LRAs may exert in the context of latency reversal, and indicate
70 a requirement for a more comprehensive understanding on the cellular effects of these treatments.
71 In cellular studies, a myriad of different LRAs and LRA combinations have shown, with
72 varying efficiencies and often in simplistic experimental models, ability to reactivate viral

73 transcription and, to some degree, expression of a reporter and/or of viral antigens[7]. However,
74 their impact on subsequent processes crucial for immune clearance, including peptide and antigen
75 presentation, and susceptibility to cytotoxic killing, has been less attentively analysed. Here, we
76 compared two different synergistically-acting LRA combinations - the iBET JQ1, paired with either
77 bryostatin-1 (Bryo), a protein kinase C agonist (PKCa) and activator of canonical NF-κB signalling,
78 or AZD5582 (AZD), an iIAP and activator of non-canonical NF-κB signalling - as potential 'shock-
79 and-kill' interventions. While both strategies shared the ability to potently reverse HIV-1 latency,
80 as previously described[8,9], they vastly differed regarding induction of cell-surface accessibility of
81 the viral Env protein and modulation of the cells´ susceptibility to cytotoxic killing. Finally, LRA
82 treatment-mediated co-induction of Nef expression antagonised increased cellular resistance to
83 killing by almost all tested latency reversal strategies, advocating for the integration of a Nef-
84 targeting approach into future 'shock-and-kill strategy' development.
85

86 **RESULTS**

87 **Bryostatin-1, despite its latency reversal activity, imposes a restriction to HIV-1 Env cell-**
88 **surface presentation**

89 In addition to presentation of peptides by MHC-I, accessibility of the HIV-1 Env glycoprotein on
90 the cell surface for binding to anti-Env antibodies is crucial for immunological visibility of HIV-1-
91 reactivating cells. We assessed how different classes and combinations of LRAs modulate HIV-1
92 Env expression and subcellular localisation, as well as cellular vulnerability to cytotoxic killing. We
93 selected bryostatin-1 and JQ1 as prototypical PKC agonist and BET inhibitor, respectively,
94 because they have been described to act synergistically[8]. The HDAC inhibitor panobinostat
95 (Pano) was included as an additional class of clinically relevant, widely used LRA[10,11]. In this study,
96 we used Jurkat E6.1 T-cells, latently infected with a full-length, replication-competent HIV-1 NL4.3
97 reporter virus bearing an optimised GFP sequence (GFP_{OPT}) fused into the V5 loop domain of

98 gp120 (Figure S1A)[12]. Three individual, clonal cell lines of Jurkat T-cells, each carrying a single
99 latent provirus per cell with known sequence and integration site (Jurkat Latent EnvGFP [JLEG]:
100 JLEG.1, JLEG.60 and JLEG.74, Table S1), expressed low-to-undetectable p24 capsid protein
101 (p24CA) and EnvGFP in the absence of stimulation (Figure 1A). Upon treatment with individual
102 LRAs, including bryostatin-1, JQ1, panobinostat, and, most pronouncedly, a combination of
103 bryostatin-1 and JQ1, JLEG.1 T-cells expressed detectable p24CA, EnvGFP, and scored positive
104 for cell-surface EnvGFP as assessed by anti-GFP immunostaining of intact cells (Figure 1A, S2A).
105 Matrix titrations of increasing concentrations of bryostatin-1 and JQ1, respectively, confirmed the
106 previously described synergy of these two molecules' ability to reverse HIV-1 latency[8] in a Bliss-
107 Independence test (Figure S1B).

108 JQ1 concentrations of 400 nM and above resulted in a significant increase from 24 to 48
109 hours for all three parameters measured (Figure 1A). In contrast, while bryostatin-1 treatment
110 induced appreciable levels of p24CA and total EnvGFP, the levels of cell-surface EnvGFP were
111 relatively low and even decreased from 24h to 48 hours post-treatment. Co-treatment with JQ1
112 appeared to reverse or prevent this downregulation (Figure 1A, S2A-C). Quantification of the
113 percentage of cell-surface EnvGFP-positive cells among p24CA-positive cells (Figure S2B)
114 confirmed that among the tested LRA strategies, only bryostatin-1 mono-treatment interfered with
115 cell-surface EnvGFP presentation over time (Figure 1B, Figure S2C). Despite displaying higher
116 cell-surface EnvGFP levels compared to the respective mono-treatments, T-cells co-treated with
117 bryostatin-1 and JQ1 showed the highest resistance to killing and poor overall clearance of
118 infected cells in an antibody dependent cellular cytotoxicity (ADCC) assay (Figure 1C). This
119 suggests that the combined treatment imposed a barrier to cytotoxic elimination of infected cells
120 that was not overcome by increased availability of the Env antigen. Indeed, bryostatin-1 and JQ1
121 co-treatment induced a marked resistance to etoposide-mediated induction of intrinsic apoptosis
122 (Figure 1D), which we hypothesised underlies the inefficiency of ADCC-mediated killing.
123

124 **Bryostatin-1 treatment induces expression of T-cell activation markers and GBPs**

125 In order to gain deeper insight into alterations of the cellular state that might underlie the observed
126 phenotypes, we performed total RNA sequencing (RNAseq) on JLEG.1 T-cells and an uninfected
127 cellular clone from the same original Jurkat culture. We noted sizable and treatment-specific
128 perturbations to the transcriptome, corresponding to high numbers of significantly up- and
129 downregulated genes (Figure 2A-B) and a relatively large overlap in differentially regulated genes
130 for the LRA treatments relative to the mock condition (Figure 2C). Importantly, the presence of a
131 provirus also considerably shaped transcriptomic responses to individual treatment strategies
132 (Figure 2D). Pathway enrichment analysis[13] revealed that bryostatin-1 increased activity for
133 pathways related to T-cell activation and effector phenotypes, including 'Interferon gamma
134 signalling' (R-HSA-877300) and 'Costimulation by the CD28 family' (R-HSA-389356), and this
135 was markedly diminished by addition of JQ1 (Figure 2E). Interestingly, analysis of the interaction
136 effect between the presence of a provirus and LRA addition indicated cooperation between
137 bryostatin-1 administration and viral reactivation to boost cholesterol biosynthesis pathways
138 (Figure 2E), possibly relating to previous observations on the influence of HIV proteins on lipid
139 metabolism[14–16].

140 When assessing the response by curated gene sets, treatment with bryostatin-1, either
141 alone or in combination with JQ1, but not JQ1 alone, markedly upregulated T-cell activation
142 markers *CD69* and *IL2RA*/*CD25*[17,18] (Figure 2F). In addition, bryostatin-1, both in the absence and
143 presence of JQ1, significantly induced *GBP2* and *GBP5* RNA levels, restriction factors previously
144 described to interfere with HIV-1 Env biosynthesis in a saturable manner[19,20]. In fact, *GBP5* was
145 identified as one of the most highly upregulated genes, both when considering global
146 transcriptomic changes across treatments (Figure S3A), and expression patterns within curated
147 gene sets of HIV-1 restriction factors (Figure 2F) and interferon signalling (Figure S3B). We
148 hypothesised that bryostatin-1 treatment, by driving T-cell activation, renders cells more resistant
149 to apoptosis, while simultaneously limiting the levels of Env presentation via the co-induction of

150 restriction factors targeting this viral protein. This would, in turn, make reactivated cells at once
151 less immunologically visible and more resistant to apoptosis-inducing cytotoxic effector
152 molecules.
153

154 **Bryostatin-1 treatment and reactivation of proviral transcription, but not AZD5582**
155 **treatment, promote T-cell activation**

156 As bryostatin-1 appeared to induce a phenotype counterproductive to immune-mediated killing of
157 infected cells, we decided to investigate the iIAP AZD5582 as a member of a different class of
158 molecules shown to synergise with BET inhibitors[9]. In contrast to AZD5582 mono-treatment,
159 treatment of all three JLEG T-cell clones with AZD5582 and JQ1 potently induced HIV-1 latency
160 reversal and high levels of cell-surface Env to an extent that was comparable to the bryostatin-1
161 and JQ1 combination (Figure 3A, S4A). The effect was also confirmed to be synergistic under the
162 Bliss-Independence model (Figure S4B).

163 As RNAseq analysis suggested that bryostatin-1 induces T-cell activation (Figure 2E-F),
164 we sought to validate this on the protein expression level, while simultaneously investigating how
165 coincident proviral reactivation shapes this response. Expectedly, treatment with bryostatin-1 and
166 the bryostatin-1 and JQ1 combination upregulated expression of the early and early-intermediate
167 activation markers CD69 and CD25 (IL2RA) in both the uninfected, parental Jurkat T-cells and
168 JLEG.1 T-cells (Figure 3B). Bryostatin-1 mono-treatment also induced the expression of the late
169 activation marker PD-L1 and the exhaustion marker PD-1, though this was dampened in these
170 systems by addition of JQ1. Induction of these activation markers was almost or completely
171 absent in treatment with AZD5582 or the AZD5582 and JQ1 combination. Importantly, the
172 activation phenotype induced by bryostatin-1 and the bryostatin-1 and JQ1 combination but not
173 by the AZD5582 and JQ1 combination was recapitulated in primary $CD4^+$ T-cells from HIV-1-
174 negative donors in that CD25, CD69, PD-L1 and PD-1 were markedly upregulated. As PD-L1

175 protects from CTL-mediated killing[21], reactivation with bryostatin-1 could be profoundly
176 counterproductive to a 'shock-and-kill' cure strategy from the perspective of cytotoxic T-cell
177 efficacy. Panobinostat, in contrast, moderately induced CD69 in JLEG.1 and primary $CD4^+$ T-cells
178 and CD25 only in the Jurkat T-cell-based systems, without affecting PD-1 or PD-L1 expression.
179 In line with a previous report in uninfected Jurkat T-cells[22], bryostatin-1 administration reduced
180 cell-surface levels of the HIV-1 receptor CD4, without altering expression of CCR5 in all T-cell
181 models tested (Figure S5A), an observation analogous to what has previously been reported in
182 macrophages[23] and is in line with an activated T-cell phenotype[24]. All tested LRAs, with the
183 exception of AZD5582 in primary $CD4^+$ T cells, reduced the expression of CXCR4, and this was
184 most striking in the bryostatin-1- containing treatments (Figure S5A). HIV-1-reactivating cells,
185 expectedly[25–29], had lower levels of cell-surface CD4 than non-reactivating cells, except in the
186 case of bryostatin-1 containing treatments where the LRA had already induced significant
187 downregulation of CD4. However, the described virus-mediated downregulation of CCR5[30,31] was
188 not observed, owing possibly to low overall levels of CCR5 expression in this system (Figure S5B).
189 Interestingly, HIV-1 reactivating cells also downregulated cell-surface CXCR4 in accordance with
190 previous reports[32,33] for all treatments except for the bryostatin-1 mono-treatment, where
191 reactivating cells displayed higher CXCR4 expression than non-reactivating cells, though the
192 reason for this is unclear.

193 Discriminating between EnvGFP-negative (non-HIV-1-reactivating) versus EnvGFP-
194 positive (HIV-1-reactivating) JLEG.1 T-cells in the same sample revealed a tendency for
195 reactivating cells to display higher levels of activation markers (Figure 3C). This was true of PD-
196 L1 in all treatments, including the mock condition, as well as CD69 (excepting the bryostatin-1
197 treatment, in which it was already maximally induced). CD25 and PD-1, additionally, were more
198 highly displayed on reactivating cells in the mock, bryostatin-1, AZD5582 and JQ1 conditions
199 (Figure 3C). This implies that not only treatment with bryostatin-1 and the bryostatin-1 and JQ1
200 combination, but also proviral reactivation itself, can drive T-cell activation programs.

201 Taken together, these data imply that the presence of the reactivating provirus *per se* can
202 drive a T-cell activation phenotype to an extent shaped partially by the LRA administered.
203 Additionally, they establish that the combination of AZD5582 and JQ1, as opposed to bryostatin-
204 1 and JQ1, at the same time enhances immunological visibility of reactivating cells by supporting
205 expression of high levels of cell-surface Env and avoids induction of an anti-apoptotic T-cell
206 activation response that would otherwise be deleterious to immune clearance.
207

208 **GBP5 expression, induced by both bryostatin-1 treatment and reactivation of proviral**
209 **transcription, is accompanied by reduced cell-surface levels of EnvGFP**

210 RNA-seq analysis provided first evidence of the bryostatin-1 treatment inducing high levels of
211 *GBP5* mRNA (Figure 2F). Given its well-documented ability to interfere with Env processing and
212 trafficking[19,20,34], we surmised that GBP5 induction may underpin the decrease in cell-surface Env
213 levels at 48 hours relative to 24 hours post-treatment with bryostatin-1 (Figure 1A-B, Figure S2).
214 Importantly, only bryostatin-1 and a reference PMA/ionomycin (PMA/Io) treatment, and not
215 AZD5582, JQ1, or the combination of these showed a reduction of Env presentation over time
216 (Figure S6A). Intracellular immunostaining for GBP5 (Figure 4A-B) confirmed the predicted
217 upregulation of GBP5 upon treatment with bryostatin-1, even at sub-nanomolar concentrations.
218 GBP5 induction also occurred with PMA/ionomycin and, to a lesser extent, during bryostatin-1
219 and JQ1 co-treatment, but not for any combination of AZD5582 and JQ1. These effects were
220 replicated in primary $CD4^+$ T cells, except in the case of panobinostat which only induced GBP5
221 in JLEG.1 T-cells (Figure 4B-D). Given that PMA/ionomycin is a known inducer of T-cell activation,
222 the data suggest that GBP5 might be upregulated as a direct consequence of the activation state.
223 Supporting this notion, other T-cell activation-inducing treatments commonly used *ex vivo* similarly
224 upregulated GBP5 in primary $CD4^+$ T-cells (Figure S6B).

225 Interestingly, HIV-1-reactivating JLEG.1 T-cells produced significantly higher levels of
226 GBP5 than non-HIV-1-reactivating T-cells from the same culture for most LRA strategies tested,
227 and importantly also under mock conditions (Figure 4C), indicating that viral reactivation may also,
228 directly or indirectly, drive GBP5 expression. GBP2 was induced by bryostatin-1 treatment, both
229 in JLEG.1 and primary $CD4^+$ T-cells, though the relative increase was more modest than GBP5
230 (Figure S6C-D). Additionally, we noted that the boosted cell-surface Env levels in the bryostatin-
231 1 and JQ1 combination condition (Figure S6A) persisted in spite of coincident GBP5 upregulation
232 (Figure 2F, 4B-D). We concluded that this likely relates to the excess of EnvGFP overcoming any
233 meaningful restriction by GBP5[34].

234 Importantly, *GBP5* knockout in the JLEG T-cell lines (Figure 4E-F, Figure S6E-F) resulted
235 in significantly higher cell-surface Env levels for all LRA regimens that induce GBP5 at 48 hours
236 post-treatment, mechanistically implicating GBP5 upregulation in the observed cell-surface Env
237 downregulation. This tendency for bryostatin-1 to limit Env antigen display via coincident
238 restriction factor upregulation is problematic for antibody-mediated detection of infected cells and
239 brings into question the usefulness of this LRA for facilitating immune-mediated clearance of the
240 viral reservoir.

241 **Bryostatin-1 and the reactivating provirus both antagonise induction of apoptosis**

242 While ADCC is initiated by effector cell recognition of antibody bound to a cell-surface antigen
243 (Env, in this case) expressed on target cells, the subsequent cytotoxic killing is mediated largely
244 by secretion of effector molecules that induce intrinsic and extrinsic apoptosis, such as Granzyme
245 B and Fas (CD95) ligand (FasL), respectively[35]**.** The relatively low ADCC efficiency (Figure 1D)
246 despite high cell-surface Env expression (Figure 1B-C), as well as the apparent reduced
247 sensitivity to intrinsic apoptosis observed in latently infected T-cells treated with the bryostatin-1
248 and JQ1 combination (Figure 1E), suggests that impaired apoptosis signalling is a major
249 contributor to the observed resistance to killing. In uninfected Jurkat T-cells, only bryostatin-1-

250 comprising treatments limited intrinsic apoptosis, compared to the mock treatment, while all LRA
251 regimens tested preserved the susceptibility of parental Jurkat cells to extrinsic apoptosis (Figure
252 5A). In stark contrast, HIV-1-infected JLEG.1 T-cells displayed resistance to cell death by both
253 intrinsic and extrinsic apoptosis upon reactivation with all treatments except AZD5582 or
254 panobinostat mono-treatment, providing a first hint for virus-mediated antagonism of apoptosis
255 induction (Figure 5A). Indeed, HIV-1-reactivating T-cells were markedly more resistant to both
256 routes of apoptosis than non-reactivating T-cells in the same sample (Figure 5B), indicating that
257 one or several viral gene products can counteract apoptosis in this system. Importantly,
258 panobinostat treatment alone, also when compared to the other LRA regimens, induced a high
259 level of apoptosis, a phenomenon described previously[36] and noticeably absent in primary $CD4^+$
260 T-cells (Figure S7A). This level of pre-existing apoptosis prior to addition of any pro-apoptotic
261 stimuli may make the results concerning apoptosis susceptibility more difficult to interpret.

262 Experiments in primary $CD4^+$ T-cells from HIV-negative donors confirmed the ability of
263 bryostatin-1 and the bryostatin-1 and JQ1 combination to decrease intrinsically induced apoptosis
264 levels (initiated here by treatment with menadione or deoxycholate). In contrast to a previous
265 report which suggested that bryostatin-1 was protective against extrinsic apoptosis[37], bryostatin-
266 1 and the bryostatin-1 and JQ1 combination slightly but significantly increased the susceptibility
267 of $CD4^+$ T-cells to extrinsic apoptosis (Figure 5C). To understand the observed phenotypes, we
268 analysed the phosphorylation and expression of key proteins involved in apoptotic signalling
269 cascades in Jurkat, JLEG.1 and primary $CD4^+$ T-cells. Although it has previously been reported
270 that bryostatin-1 administration triggers the phosphorylation and associated hyperfunction of the
271 anti-apoptotic BCL2 protein[37], we were unable to reproduce this finding (Figure 5D). In contrast,
272 the phosphorylation of the pro-apoptotic Bad protein at Ser112 increased upon treatment with
273 bryostatin-1 and the bryostatin-1 and JQ1 combination across all T-cell models tested.
274 Phosphorylation of Bad is associated with its hypofunction via cytosolic sequestration by 14-3-3[38].
275 Interestingly, treatment with bryostatin-1 and the bryostatin-1 and JQ1 combination significantly

276 increased the expression of CD95 (Fas) on the surface of primary $CD4^+$ T-cells, likely
277 underpinning the observed increase in extrinsically induced apoptosis in these cells. In the same
278 system, bryostatin-1 administration very slightly reduced expression of the anti-apoptotic BCL-xL
279 protein, but also moderately increased levels of the anti-apoptotic MCL-1 protein (Figure S7B). In
280 contrast, no meaningful change was observed for any combination of AZD5582 and JQ1.

281 Overall, this provides support to the notion that treatment with bryostatin-1 and the
282 bryostatin-1 and JQ1 combination, but not with AZD5582 and JQ1, impedes intrinsic apoptosis
283 pathways. Concurrently, we identified a role of the reactivating provirus in blocking both intrinsic
284 and extrinsic apoptosis in the context of infected cells. This not only highlighted the utility of the
285 AZD5582 and JQ1 combination strategy as more conducive to 'shock-and-kill', but also made
286 clear how viral resistance to cell death signalling poses an additional hurdle that would likely have
287 to be overcome for a maximally effective cure strategy.

288

289 **Blocks to ADCC after bryostatin-1 treatment are unrelated to ADCC co-factor modulation**

290 Beyond the availability of cell-surface antigens and relative functioning of apoptotic pathways, an
291 additional factor influencing ADCC-mediated killing could be downregulation of ADCC co-factors
292 from the cell surface, including CD48, SLAMF6, PVR. However, bryostatin-1 treatment
293 significantly upregulated the expression of CD48 in all T-cell types tested, and increased SLAMF6
294 expression in Jurkat and JLEG.1 cells (Figure 6A). Addition of JQ1 to Bryostatin prevented or
295 reduced these upregulations, but did not reduce the expression level to below that of the mock-
296 treated samples. While PVR levels were not meaningfully altered by bryostatin-1 mono-treatment
297 or the bryostatin-1 and JQ1 combination in Jurkat cells, treatment with JQ1, AZD5582 and JQ1,
298 and panobinostat modestly downregulated this cell-surface receptor. For JLEG.1 T-cells, PVR
299 was more clearly downregulated in the bryostatin-1 and JQ1 condition, likely owing to HIV-1-
300 reactivating cells showing lower cell surface PVR levels than non-reactivating cells (Figure 6B).
301 In primary $CD4^+$ T-cells, PVR levels were markedly upregulated, for both bryostatin-1 and the

302 bryostatin-1 and JQ1 combination (Figure 6A). Bryostatin-1 also slightly upregulated the
303 expression of HLA-E, a negative regulator of NK cell-mediated killing[39], in Jurkat T-cells, although
304 the combination of bryostatin-1 and JQ1 specifically led to significantly higher levels of this
305 inhibitory factor of ADCC in primary $CD4^+$ T-cells (Figure 6A). Taken together, these data indicate
306 that low levels of ADCC observed in the bryostatin-1-containing treatments likely cannot be
307 ascribed to ADCC co-factor modulation.
308

309 **Knockout of the viral *nef* gene increases susceptibility of HIV-1-reactivating T-cells to**
310 **apoptosis and ADCC-mediated killing**

311 HIV-1 Nef has been described to exert both anti-apoptotic[40–42] and pro-apoptotic[43,44] effects, likely
312 dependent on cellular and viral context. To test if Nef underpins the resistance of HIV-1-
313 reactivating T-cells to apoptosis, we generated CRISPR/Cas9-mediated knockouts of the HIV-1
314 *nef* gene in the proviruses of the JLEG T-cell lines (Figure 7A). This allowed for an isogenic
315 comparison of wild-type and *nef*-deficient proviruses situated at the identical integration site. As
316 expected, *nef* knockout prevented the Nef-mediated downregulation of cell-surface MHC-I[45]
317 (Figure 7B) and partially rescued cell-surface CD4 levels (Figure S8A)[46] on HIV-1-reactivatingT-
318 cells, functionally validating *nef* knock-out. CD69 expression, however, as a marker for T-cell
319 activation, appeared to be largely independent of Nef expression (Figure S8A). Interestingly, for
320 most, but not all LRAs tested, loss of Nef partially reduced the levels of HIV-1 reactivation as
321 measured by viral p24CA expression (Figure 7C, left panel), but markedly increased relative cell-
322 surface levels of EnvGFP for all non-bryostatin-1-containing LRA treatments in two of three JLEG
323 clones (Figure 7C right panel, Figure S8B).

324 Loss of Nef significantly improved the susceptibility of HIV-1-reactivating T-cells to intrinsic
325 apoptosis, though it did not completely overcome the observed resistance relative to non-
326 reactivating cells (Figure 7D). However, in the case of extrinsically induced apoptosis, knockout

327 of *nef* appeared to completely ablate the resistance of HIV-1-reactivating T-cells to this apoptotic
328 signalling mode in all treatments except for panobinostat. Taken together, these results
329 demonstrate the ability of Nef to interfere with both intrinsic and extrinsic apoptotic signalling
330 pathways in the context of HIV-1 reactivation. In addition, we observed a pattern of higher levels
331 of pBad S112 in HIV-1-reactivating, compared to non-reactivating T-cells (Figure S8C).
332 Surprisingly, *nef* knockout had no effect on this phenotype, though triggering Bad phosphorylation
333 has been described as a key mechanism by which Nef blocks intrinsic apoptosis[40].

334 As knock-out of *nef* increased the susceptibility of reactivating T-cells to apoptosis and
335 enhanced cell-surface Env levels, we investigated whether it may also bolster ADCC responses.
336 As expected[47,48], deletion of *nef* resulted in higher ADCC inhibitory factor HLA-E and ADCC co-
337 factor PVR levels in HIV-1-reactivating cells (Figure 7E), where the absence of a complete rescue
338 can likely be ascribed to Vpu in this system. For all treatments except panobinostat, *nef* knockout
339 resulted in a significant increase in the percentage of p24CA-positive cells killed in the three JLEG
340 cell lines in an ADCC assay (Figure 7F, left panel, Figure S8D). Crucially, the combination of
341 AZD5582 and JQ1, in the context of *nef* knockout, resulted in the largest total reduction in infected
342 cells for all three JLEG clones (Figure 7F, right panel, Figure S8D). This observation not only
343 highlights the role played by Nef in the evasion of immune clearance by latently infected cells, but
344 also outlines how the synergistically acting iIAP and iBET combination, paired with targeted Nef
345 antagonism, could form the basis of a novel approach to HIV cure strategies that emphasises both
346 the efficacy of latency reversal and the potency of host immune function in clearing the latent
347 reservoir.

348

349 **DISCUSSION**

350 Assessment of HIV latency reversal efficacy and dynamics has largely been performed in cells
351 bearing minimal proviral reporter systems, such as the JLat model[49–51], or proviruses often lacking

352 both *nef* and/or *env*[52–56]. The vast majority of these cellular studies have investigated the 'shock'
353 component of 'shock-and-kill' by assessing reporter expression following latency reversal, while
354 not many have assessed the 'kill'[57]. Due to the relative rarity of infected cells in peripheral blood
355 from PLWH under ART, *ex vivo* analyses are typically restrained to quantifying changes of intra-
356 or extracellular viral RNA levels ('shock') and proviral DNA levels ('kill) at bulk level[58–60]. While
357 these investigations are valuable, they cannot establish the percentage of cells reactivating HIV-
358 1 transcription among all latently infected cells, and do not capture events modulating immune
359 clearance upon latency reversal, such as Nef-mediated downregulation of MHC-I or cell-surface
360 presentation of Env glycoproteins. The JLEG model of latency developed here is based on a full-
361 length provirus with all viral genes expressed and functional. It more closely models authentic
362 HIV-1 reactivation and allows tracking of both Env expression and cell-surface presentation at
363 single-cell level. Importantly, with each cell containing a single provirus, this system allows
364 quantification of relative efficiency of elimination upon a given treatment, something that is not
365 achievable when using samples from PLWH. While the three T-cell clones used in this study do
366 not represent the full spectrum of the HIV-1 reservoir heterogeneity present *in vivo*, they all shared
367 latency reversal characteristics and responses to LRA treatment, indicating that results obtained
368 are not specific to one specific integration site.

369 While a plethora of individual LRAs have been described to date[7,61], combinations of
370 compounds represent an opportunity to achieve synergy and target a more diverse population of
371 proviruses whose reactivation may require different mechanisms, while potentially allowing the
372 use of lower concentrations *in vivo*. In addition to confirming the reportedly synergistic and potent
373 ability of the combination of the iIAP AZD5582 and iBET JQ1 to reverse latency[9], our data
374 establish that it is uniquely able to prevent T-cell activation, maintain full susceptibility to apoptosis
375 induction, result in high levels of Env expression and, as a consequence induce the highest
376 elimination rates of all treatments tested. As a bipartite strategy, 'shock-and-kill' necessitates that
377 equal weighting be given to both the endeavour to reactivate transcription of latent proviruses and,

378 in a second step, eliminate virus-infected cells. Mechanistically, knowledge regarding how
379 treatment with LRAs, and the consequences of reactivation of proviral gene expression, affects
380 cellular states, is limited. Furthermore, a better understanding of how the resulting perturbations
381 modulate susceptibility to immune-mediated killing is also needed. T-cell activation, as measured
382 by established activation markers, was clearly induced by bryostatin-1-containing treatments but
383 not for any combination of AZD5582 and JQ1. This activation phenotype was also driven by
384 proviral reactivation, as determined by discriminating between HIV-1-reactivating and non-
385 reactivating cells in the same sample, and has been described to render T-cells refractory to pro-
386 apoptotic stimuli[62–65], thereby making them less susceptible to immune clearance. Of note was
387 the upregulation of PD-L1 in response to the reactivating provirus, independent of the LRA
388 applied, and to bryostatin-1 treatment directly (as evidenced in uninfected Jurkat T-cells). Of note,
389 PD-L1 expression dampens cytotoxic $CD8^+$ T-cell responses, a phenomenon best described in
390 the context of cancer[21], and therefore should not be boosted by an ideal LRA. To our knowledge,
391 PD-L1 upregulation in the context of HIV-1 infection or replication as a direct consequence of
392 intracellular viral components, rather than exogenous addition of HIV-1-derived TLR agonists [66]
393 or induction of type I IFN signalling[67], has not been described before, suggesting that this may be
394 an unexplored route by which HIV-1-infected cells evade CTL recognition. Our observation that
395 bryostatin-1 upregulates key T-cell activation markers in all analysed T-cell models is in line with
396 several reports[68,69] , some of which however demonstrated limited proliferative responses,
397 pointing towards incomplete T-cell activation by Bryostatin alone[68].

398 Presentation of cell-surface Env as the only extracellularly accessible viral antigen is a
399 crucial factor for ADCC responses, which hinge on the binding of anti-Env antibodies and the
400 subsequent recruitment of effector cells[70,71]. However, we identified the HIV-1 restriction factor
401 GBP5 to be induced by bryostatin-1 administration and in response to a reactivating provirus,
402 though not as a direct result of AZD5582 and JQ1 combination treatment. Given its documented
403 ability to interfere with biosynthesis and intracellular trafficking of HIV-1 Env during *de novo*

404 infection[19,20,34], we hypothesised high GBP5 expression in the context of latency reversal would
405 be accompanied by reduced cell-surface Env levels. This was confirmed and *GBP5* knockout
406 experiments established a causal relationship between GBP5 expression and reduction of cell-
407 surface Env, demonstrating that at least a part of the bryostatin-1-imposed suppression of cell-
408 surface Env presentation is mediated by induction of this restriction factor. It is important to note
409 that the degree of GBP5 induction in the context of the combination of bryostatin-1 and JQ1 was
410 insufficient to fully impede HIV-1 Env cell-surface presentation, an observation most likely
411 explained by saturation of the restriction factor by high levels of Env expression upon reactivation
412 by this potent combination[34]. It will be interesting to investigate by which mechanism the
413 combination of AZD5582 and JQ1 suppresses GBP5 expression, and whether other Env-targeting
414 ISGs, which would otherwise interfere with cell-surface Env presentation, may be equally
415 suppressed.

416 Recent efforts to sensitise latently infected cells to apoptosis centre on inhibiting the anti-
417 apoptotic BCL2 protein[72–74]. Notably, the IAP antagonist AZD5582, beyond reversing latency, can
418 also sensitise cells to apoptosis by binding to and triggering the degradation of the anti-apoptotic
419 proteins cIAP1 and XIAP, a phenotype described in the context of human pancreatic cancer[75]. As
420 such, AZD5582 and related molecules have the potential to perform a dual function in HIV cure
421 approaches. In contrast to AZD5582-containing treatments, bryostatin-1-containing treatments
422 reduced the ability of T-cells to cleave caspase-3 upon administration of inducers of intrinsic
423 apoptosis. While this refractoriness to apoptosis inducers is potentially linked to the initiation of T-
424 cell activation by bryostatin-1, it was accompanied by phosphorylation of Bad at S112, a post-
425 translational modification known to induce the hypofunction of this pro-apoptotic protein by
426 facilitating its cytosolic sequestration via 14-3-3[38,76]. Bad phosphorylation and function depend on
427 the MAPK/ERK and PI3K/Akt signalling pathways[77,78]. Both of these are directly involved in T-cell
428 activation responses[79–83], providing a likely mechanistic link between T-cell activation, Bad
429 phosphorylation and lowered responsiveness to apoptosis inducers. Interestingly, bryostatin-1

430 has previously been described to block apoptosis by inducing phosphorylation and subsequent
431 hyperfunction of the anti-apoptotic BCL2 protein at S70[37], though this was not reproducible in our
432 investigation. Importantly, a flow cytometric analysis differentiating LRA-treated cells according to
433 their p24CA positivity status uncovered a propensity of HIV-1-reactivating cells to evade both
434 intrinsic and extrinsic apoptosis, indicating a contribution of a co-induced, viral component in
435 counteracting apoptosis induction. The combination of these bryostatin-1-induced blocks to and
436 viral antagonism of apoptosis likely underpins the low levels of ADCC-mediated killing observed
437 for bryostatin-1 containing conditions, though we concluded that this was likely not due to a
438 modulation of ADCC co-factors by the LRA.

439 The HIV-1 viral accessory protein Nef is a multi-functional protein, perhaps best
440 characterised for its ability to downregulate cell-surface CD4 and MHC-I levels[45,46]. It also appears
441 to act both pro- and anti-apoptotically, depending on context[40–44]. By downregulating MHC-I, Nef
442 allows for immune evasion by cytotoxic lymphocytes, while its downregulation of PVR [47] and CD4
443 [84] serves to confound humoral immunity. Our findings demonstrating Nef as a factor reducing cell-
444 surface Env presentation are reminiscent of early work demonstrating Nef-modulated efficiency
445 of Env-dependent syncytia formation[85]. The exact role of Nef in modulating cell-surface levels of
446 Env remains somewhat controversial, however, with early studies suggesting that Nef expression
447 leads to less presentation of Env[86] and others suggesting that Vpu, rather than Nef, is responsible
448 for limiting cell-surface Env[84]. What has become apparent is that, while cell-surface Env is required
449 for ADCC, the efficacy of cytotoxic killing hinges on the binding of anti-Env IgG serum antibodies
450 and this, in turn, is dependent on Env conformation and CD4-Env binding[70,87,88]. Because the CD4-
451 bound, “open” conformation of Env exposes epitopes readily recognised by antibodies in sera
452 from PLWH[87], downregulation of CD4 by Nef shifts Env toward the more ADCC resistant "closed"
453 conformation, thereby impeding ADCC[84,89]. However, while all prior work has been done in the
454 context of acute infection, our report is the first to describe the role of Nef in modulating cell-
455 surface Env in the context of latency reversal. In addition to diminishing antigen visibility, this

456 work is the first to provide evidence of Nef protecting T-cells from intrinsically and extrinsically
457 induced apoptosis in the context of latency reversal. Importantly, these Nef-mediated phenotypes
458 culminated in Nef-mediated protection from antibody-dependent cytotoxic killing, establishing Nef
459 as a key, yet overlooked antagonist of 'shock-and-kill' strategies. Indeed, it is likely that Nef-
460 mediated antagonism of ADCC is driven by a combination of PVR downregulation, apoptosis
461 inhibition, cell-surface Env presentation limitation and prevention of the ADCC-sensitising,
462 "opening" CD4-Env interaction by degradation of CD4.

463 Together, this work advocates for a careful preclinical assessment of biological
464 consequences, and efficacies both at 'shock' and 'kill' level, of LRA treatment before prioritisation
465 for clinical studies. As an example, a phase I clinical trial in aviremic PLWH found that bryostatin-
466 1 administration, while well tolerated, failed to induce a detectable increase in HIV RNA levels[90].
467 An analogous study investigating panobinostat demonstrated a measurable, treatment-induced
468 upregulation of unspliced, cell-associated viral RNA but no reduction in the overall viral reservoir[10].
469 These results are in line with those presented in this study, where we found that bryostatin-1 had
470 limited efficacy when administered as mono-treatment. Panobinostat, in addition, triggered robust
471 latency reversal, but underperformed relative to the AZD5582 and JQ1 combination where ADCC-
472 mediated elimination efficacy was concerned. In line with this, work from our group[91] and others
473 [92] has indicated that panobinostat may dysregulate normal function in immune cells. Possibly, this
474 could also impact the susceptibility of cells to cytotoxic killing, even in the absence of a functional,
475 ant-apoptotic Nef protein.

476 As a way forward, we propose synergistic latency reversal with an iIAP and iBET
477 (AZD5582 and JQ1, or related molecules), coupled with ablation of the viral Nef protein, as a
478 blueprint for the development of a cure strategy merging potent HIV-1 reactivation, optimal
479 immunological visibility and full susceptibility to immune-mediated killing of infected cells. Other
480 tested individual and combinatorial latency reversal strategies suffered from one or several
481 insufficiencies and should therefore be deprioritised regarding *in vivo* testing. Notably, the

482 simultaneous administration of iBETs and iIAPs *in vivo* has been reported to be well-tolerated in
483 a small study of SIVmac251-infected macaques[93] and induced favourable immunomodulatory
484 effects as well as restriction of tumor growth in a mouse model of pancreatic cancer[94], indicating
485 good translational potential of this strategy. While some headway has been made in the
486 development of Nef inhibitors and degraders[95–97] and they have shown promise in potentiating
487 immune-mediated killing of infected cells[98], further research is needed in the context of 'shock-
488 and-kill' HIV cure approaches. Combining synergistic latency reversal with Nef inhibition,
489 therefore, represents a novel approach to HIV cure that should be investigated in the context of a
490 more complex system, such as a small animal model of HIV-1 infection.
491

492 **MATERIALS AND METHODS**

493

494 Reagents
495 Bryostatin-1 (Bryo, Merck), (+)-JQ1 (JQ1, Universal Biologicals), AZD5582 (AZD, Sigma-Aldrich),
496 panobinostat (Pano, Cayman Chemical), Phorbol 12-myristate 13-acetate (PMA, InvivoGen),
497 Ionomycin (Io, InvivoGen), etoposide (Merck) were solved in dimethyl sulfoxide (DMSO, Stratech
498 Scientific). Phytohaemaglutinin P (PHA) was obtained from Invivogen, while human recombinant
499 IL-2 (IL-2) and CD3/CD28 Dynabeads™ (anti-CD3/CD28 beads, Gibco) were obtained from
500 STEMCELL and Thermo Fisher, respectively. The anti-CD3/CD28 beads were used according to
501 the manufacturer's recommendations (1:1 bead-to-cell ration). Efavirenz (EFV) was obtained
502 from the NIH AIDS Reagent program. Mouse anti-Human CD95 (clone DX2) and recombinant
503 Protein G' were purchased from BD Biosciences and Sigma-Aldrich, respectively. Protein G was
504 resuspended in sterile water (Merck) and stored at -20°C. Sodium deoxycholate (Merck) was

505 dissolved in PBS (Merck) and frozen at -20°C. Menadione (Merck) was dissolved in N,N-
506 Dimethylformamide (DMF, Sigma-Aldrich).
507
508 Cell lines and primary cells
509 Cells were cultured at 37°C in a humidified incubator with 5% CO2. HEK293T cells were obtained
510 from ATCC and cultured in Dulbecco's modified Eagle's medium (DMEM, Merck) supplemented
511 with 10% heat-inactivated fetal calf serum (FCS, Merck), 100 IU/ml Penicillin/Streptomycin and 2
512 mM L-Glutamine (Thermofisher). Jurkat E6.1 T-cells were obtained from the NIH AIDS Reagents
513 Program and cultured in RPMI 1640 (Merck) with 10% heat-inactivated fetal calf serum (FCS,
514 Merck), 100 IU/ml Penicillin/Streptomycin, 2 mM L-Glutamine, 1X MEM non-essential amino acids
515 and 1mM sodium pyruvate (both Thermo Fisher). Primary $CD4^+$ T-cells were isolated from blood
516 (buffy coats from anonymous, HIV-1-negative donors) using the EasySep™ Direct Human CD4+
517 T-Cell Isolation Kit (STEMCELL Technologies) according to the manufacturer's instructions.
518 Human PBMCs were isolated using Ficoll-Hypaque (Pancoll, PAN Biotech) centrifugation.
519 Primary $CD4^+$ T-cells were cultured in the same medium as Jurkat E6.1 T-cells, as were all JLEG
520 T-cell lines, unless otherwise stated. JLEG T-cells were cultured in the presence of 100nM EFV
521 to prevent viral spread in culture.
522

523 Molecular cloning, lentiviral vectors and CRISPR/Cas9 knockout
524 The HIV NL4.3 V5.3 EnvGFP infectious molecular clone was created following [12], with the reporter
525 protein and GS-linkers inserted 3' of the third codon of the V5 loop domain of Env in the pNL4.3
526 plasmid (NIH AIDS Reagents Program). Knockouts in JLEG T-cells were obtained by lentiviral
527 transduction using the LentiCRISPRv2 vector system (Addgene #52961). Sequences encoding a
528 non-targeting, control sgRNA (5'-AAAAAGCTTCCGCCTGATGG-3') and an sgRNA targeting
529 human *GBP5* (5'-CATTACGCAACCTGTAGTTG-3') were taken from the published sequences in

530 the Brunello human knockout CRISPR library[99]. The *nef*-targeting sgRNA (5'-
531 ATTGGTCTTAAAGGTACCTG-3') was generated using the CHOPCHOP webtool[100,101]. The
532 sequences were inserted into the LentiCRISPRv2 vector using the *BsmB*I cloning site and the
533 insertion was validated by Sanger sequencing.
534

535 LRA treatment
536 Cells were treated with bryostatin-1 (4nM) in the presence or absence of JQ1 (400nM), JQ1
537 (400nM) alone, AZD5582 (10nM) in the presence and absence of JQ1 (400nM), panobinostat
538 (50nM) or a combination of PMA (0.01µg/ml) and Io (1µg/ml) for the indicated time points, unless
539 stated otherwise. DMSO was used as a mock (or 'vehicle') control at a final concentration of
540 0.005% (v/v).
541

542 Antibodies
543 All primary and secondary antibodies used in this study for both flow cytometry and
544 immunoblotting, as well as the dilutions employed, are listed in Table S2.

545 Flow cytometry
546 For cell-surface protein detection, cells were immunostained in FACS buffer (1% BSA, Gibco;
547 0.05% sodium azide, Thermofisher; in PBS) at 4°C in the dark for 30min. Cells were fixed in 4%
548 paraformaldehyde (PFA, VWR) in PBS. For intracellular protein detection, PFA-fixed cells were
549 either simultaneously immunostained and permeabilised in 0.1% Triton-X100 (Perkin Elmer) for
550 20min at RT, or first permeabilised in 90% methanol (Thermo Fisher) in dH2O for 15min on ice,
551 followed by immunostaining for 30min at RT. Cells were incubated with appropriate secondary
552 antibodies. A list of the detection antibodies used in this study is provided as supplementary table
553 1. Cell-surface EnvGFP was detected using an anti-GFP antibody conjugated to eFluor660 (clone
554 5F12.4, eBioscience) at a dilution of 1:300. Samples were analysed on a BD FACS Celesta (BD

555 Biosciences) or a Cytek Aurora (Cytek) flow cytometer. Analysis of FCS files was performed using
556 FlowJo v10 (FlowJo, LLC). JLEG.1 T-cells express very low levels of GBP5 without stimulation
557 (typically 2-3% of cells positive) therefore upregulation of GBP5 was quantified as the change in
558 the percentage of cells positive. In $CD4^+$ T-cells, high levels of GBP5 are expressed at baseline
559 (Figure 4B), therefore GBP5 was quantified as the change in MFI.
560

561 Generation of HIV-1 virions and lentiviral particles

562 To generate authentic HIV-1 virions and pseudoviral particles, corresponding plasmids were
563 transfected into HEK293T cells using the CalPhos™ Mammalian Transfection Kit (Takara). For
564 generation of pseudoviral particles, the corresponding transfer plasmid was co-transfected with
565 the packaging plasmid psPAX2 (Addgene #12260) and the VSV-G-encoding vector. 48h and 72h
566 post-transfection, supernatant was harvested and filtered using a Stericup vacuum filtration
567 system with a 0.22µm PES filter (Millipore). Viral particles were concentrated by ultracentrifugation
568 over a 20% sucrose (Sigma-Aldrich) cushion at 152,982 x *g* at 4°C for 90min (SW 32 Ti swinging-
569 bucket rotor, Beckman Coulter), resuspended in full RPMI medium and stored at -80°C. The HIV
570 NL4.3 EnvGFP used for generation of JLEG cell lines was pseudotyped with vesicular stomatitis
571 virus glycoprotein (VSV-G)[102].

572 Generation of latently infected Jurkat T-cell lines (JLEG)

573 Jurkat E6.1 T-cells were infected with VSV-G-pseudotyped HIV NL4.3 V5.3 EnvGFP at an MOI
574 of 0.1 for six days, resulting in approximately 10% EnvGFP-positive cells as determined by flow
575 cytometry. From that time point on, cells were maintained in medium containing 100nM EFV to
576 prevent viral spread. Virtually no EnvGFP signal was detectable after 14 days. Cells were seeded
577 into 96-well plates at a concentration of 0.5 cells per 100 ul per well and cultured for three weeks.
578 The resulting single-cell clones were screened for the presence of a single integrated provirus per

579 cell using nested *Alu-gag*, R-U5 PCR[103]. Positive clones were expanded and termed Jurkat Latent
580 EnvGFP (JLEG) cells.
581
582 Analysis of JLEG integration sites and proviral sequences
583 To determine the viral integration site and full proviral sequence in three provirus-positive clones
584 used in this study, total genomic DNA was extracted and DNAseq libraries were prepared using
585 the KAPA HyperPrep kit (Roche). To target library fragments comprising viral DNA and host-virus
586 junctions, probe-based enrichment was performed using the KAPA HyperCap kit (v3.2, Roche),
587 along with custom biotinylated probes to the viral DNA sequence. Libraries were quantified using
588 a Qubit 3 fluorometer (Thermofisher) and size distributions of library fragments were validated
589 using an Agilent TapeStation automated capillary electrophoresis machine. Libraries were
590 multiplexed and sequenced on an Illumina Miseq platform. Dual indexed, paired end (2x150bp)
591 reads were generated with a targeted read-depth of at least two million reads per original sample.
592 Raw paired-end sequencing reads were aligned to the Homo sapiens reference genome
593 (GRCh38) using Nvidia Clara Parabricks (v4.0.1). The Parabricks fq2bam workflow was used to
594 accelerate the alignment process on GPUs, generating sorted and indexed BAM files. Following
595 alignment, viral integration events were detected using the GRIDSS VIRUSBreakend
596 pipeline[104,105]. This tool employs single breakend variant calling to identify viral DNA presence and
597 genomic integration sites with high sensitivity. The resulting VCF files were then filtered using
598 bcftools to isolate unique integration sites[106]. Strict filtering criteria were applied to retain only
599 variants matching the 5' and 3' Long Terminal Repeat (LTR) boundaries of the HXB2 reference
600 genome (NC_001802.1), ensuring the capture of integration junctions regardless of viral
601 orientation. For this step, the HXB2 reference genome (NC_001802.1) was utilised rather than
602 the experimental NL4.3 strain, as it is the annotated standard available in the VIRUSBreakend
603 reference database.

604 Immunoblotting

605 Cells were lysed using either M-PER™ Mammalian Extraction Reagent or RIPA Lysis and
606 Extraction Buffer (both Thermofisher), supplemented with 1X Halt™ Protease Inhibitor Cocktail
607 and EDTA and 1X Halt™ Phosphatase Inhibitor Cocktail (all ThermoFisher) for 30min at 4°C. The
608 insoluble fraction was pelleted at 20,000*g* for 10min at 4°C and the supernatant mixed with 4X
609 SDS lysis buffer (0.625M Tris/HCl pH6.8, Sigma-Aldrich; 8% SDS, Cytiva; 400mM β-
610 mercaptoethanol, Universal Biologicals; 40% glycerol, Thermo Fisher; 0.08% bromophenol blue,
611 VWR) to a final concentration of 1X. Samples were heated at 95°C for 10min and stored at -20°C.
612 Immunoblotting and subsequent quantification of protein abundance was performed as previously
613 described [91].

614 Infection and lentiviral transduction

615 Infection of Jurkat E6.1 T-cells and lentiviral transduction of JLEG T-cells were performed by
616 spinoculation. In brief, cells were mixed with concentrated lentiviral stocks and centrifuged at
617 1,000 x *g*, 37°C for 90min. Treatment with puromycin (Sigma-Aldrich) at 1µg/ml started three days
618 post infection for ten days.

619 Apoptosis assays

620 In T-cell lines, intrinsic and extrinsic apoptosis was induced by cultivation of cells in medium
621 containing 20µM etoposide for 16h and 6.25µg/ml anti-CD95 (clone DX2) with 3.25 µg/ml
622 recombinant Protein G' for 5h, respectively. Apoptosis was induced after treatment with indicated
623 LRAs for 24h. For primary $CD4^+$ T-cells, apoptosis was induced by cultivation in medium
624 containing 15µM menadione or 600µM deoxycholate (intrinsic apoptosis), or 6.25µg/ml anti-CD95
625 with 6µg/ml recombinant Protein G' (extrinsic apoptosis) for 24 hours. Cleaved, active Caspase 3
626 as an indicator of apoptosis was quantified flow cytometrically by anti-active Caspase 3
627 immunostaining (clone C92-605.rMAb, BD Biosciences). During apoptosis induction, cells were
628 cultured in the absence of sodium pyruvate and L-Glutamate as these may act as reducing agents.

629

630 Preparation and sequencing of RNAseq libraries

631 Two million JLEG.1 T-cells and cells derived from an uninfected clone were mock-treated, or
632 treated with bryostatin-1 (4nM), JQ1 (400nM) or a combination of bryostatin-1 and JQ1 for 24h.
633 Cell lysates were inactivated in 300µl TRI Reagent (Zymo Research) for 10min at RT. RNA was
634 extracted using Direct-zol RNA Miniprep kit (Zymo Research) and quantified using the Qubit™
635 RNA High Sensitivity kit and the Qubit 4 Fluorometer (Thermo Fisher). 400ng of RNA per sample
636 was used to generate total RNA-sequencing (RNAseq) libraries using the Stranded Total RNA
637 Prep with Ribo Zero Plus library prep kit (Illumina). The libraries were quality-controlled using a
638 4200 TapeStation device and the D1000 DNA ScreenTape kit (Agilent) and sequenced to a depth
639 of 50 million reads per library on a NovaSeq 6000 (Illumina) as 75 nucleotide paired-end reads.

640

641 ADCC assays

642 JLEG T-cells (target cells) were treated with the respective LRAs or LRA combinations for 24h,
643 resuspended in serum-free RPMI containing a 1:1000 dilution of 1mM CellTracker™ Deep Red
644 (Thermo Fisher) and incubated at 37°C for 15min. After washing with PBS to remove remnants of
645 LRAs in the supernatant, stained cells were seeded at a concentration of 10^6 cells/ml in 100µl in
646 a 96-well plate. After addition of pooled anti-HIV sera (#3957, NIH AIDS Reagent Program, final
647 dilution 1:100), freshly isolated PBMCs from anonymous, HIV-uninfected donors (effector cells)
648 were added to target cells to a final effector:target cell ratio of 1.5:1. Cocultures without HIV serum
649 served as a reference. Cocultures were centrifuged at 300g for 1min to maximise contact between
650 effector and target cells and incubated for 4h at 37°C, 5% CO2. Following fixation, cells were
651 immunostained for intracellular HIV-1 p24 expression (clone KC57, Beckman Coulter). The
652 measures of ADCC efficiency were calculated as follows::

653

654 Reduction in p24CA-positive cells (%) =

655 [(% p24CA$^+$ target cells$_{\text{No anti-HIV-1 sera}}$ - % p24CA$^+$ target cells$_{\text{1:100 anti-HIV-1 sera}}$)] / % p24CA$^+$ target

656 cells$_{\text{No anti-HIV-1 serum condition}}$ x 100

657

658 The total reduction in infected cells was calculated as follows:

659

660 ADCC elimination efficiency (%) =

661 (Reduction in p24CA-positive cells % /100) x Average % p24CA$^+$ cells for treatment condition

662

663

664 Data analysis

665 FASTQ files from the sequencing output were aligned to GRCh38 v109 (Ensembl) using STAR[107].

666 Gene counts were assigned using Rsubread[108] and downstream analysis was performed using

667 DESeq2[109] within the R programming language, v4[110]. The code is available at

668 https://github.com/GoffinetLab/HIV_Synergistic-Latency-Reversal-study and raw sequencing

669 data will be made available on the NCBI GEO database.

670

671 Statistical analysis

672 All data was processed using R v4[110] and graphics were produced using the ggplot2[111] and

673 pheatmap[112] packages. Statistical analysis was performed using the rstatix package[113] and Bliss-

674 Independence testing for synergy between bryostatin-1 and JQ1 was performed using the BIGL

675 package[114]. Bliss-Independence testing of synergy between AZD5582 and JQ1 was performed

676 by first subtracting the value for a given parameter observed in the mock treatment from the value

677 observed for each LRA treatment respectively. Thereafter, the expected combination effect was

678 determined with the corrected values using the formula Effect$_{\text{(expected, AZD5582+JQ1)}}$ = E$_{\text{(observed, AZD5582)}}$

679 + $E_{(observed, JQ1)}$ - $E_{(observed, AZD5582)}E_{(observed, JQ1)}$. Bliss excess was then calculated using the formula:
680 Bliss excess = $Effect_{(observed, AZD5582+JQ1)}$ - $Effect_{(expected, AZD5582+JQ1)}$, with positive and negative values
681 indicating synergy and antagonism respectively. Statistical significance was then determined by
682 comparing the values for $Effect_{(observed, AZD5582+JQ1)}$ and $Effect_{(expected, AZD5582+JQ1)}$ using a Wilcoxon
683 rank-signed test. Code used is available at https://github.com/GoffinetLab/HIV_Synergistic-
684 Latency-Reversal-study.
685
686 Ethics
687 Withdrawal of blood samples from anonymous, HIV-negative human donors and cell isolation
688 were conducted with approval of the local ethics committees (Ethical review committee of Charité
689 Berlin, vote EA4/167/19; NHSBT, acc. M252).
690
691 **RESOURCE AVAILABILITY**
692 *Lead contact.* Further information and requests for resources should be directed to and will be
693 fulfilled by the lead contact, Christine Goffinet, christine.goffinet@lstmed.ac.uk.
694 *Materials availability*. Cell lines will be provided on reasonable request.
695 *Data and code availability*. Code used in this study is available at
696 https://github.com/GoffinetLab/HIV_Synergistic-Latency-Reversal-study.
697 Raw sequencing data will be made available on the NCBI GEO database.
698
699 **AUTHOR CONTRIBUTIONS**
700 DP generated the majority of the data. STH conducted the integration site analysis of the
701 proviruses of the three JLEG clones. BA generated the recombinant NL4.3 Env.GFP_{OPT} molecular
702 clone. JJ and DP provided technical assistance. OC provided essential reagents. CG supervised

703 the work. DP and CG wrote the manuscript. All authors read, edited, and approved the
704 manuscript.
705
706 **DECLARATION OF INTERESTS**
707 Authors DP and CG are inventors on a pending patent application covering the combination
708 described in this study.
709

710 **ACKNOWLEDGEMENTS**

711 We thank the anonymous blood donors for providing their blood for research. We thank Valerie
712 Bosch and the NIH AIDS Research & Reference Reagent Program for providing essential
713 reagents. We thank the Genomics Platform of the Berlin Institute of Health for next-generation
714 sequencing. This work was supported by funding to C.G. by Berlin Institute of Health (BIH); by
715 Hector Foundation, project M2101; by DFG priority program 1923 “Innate Sensing and Restriction
716 of Retroviruses,” grant GO2153/4; by DZIF, TTU HIV, grant 04.820 to C.G., by a Professorship
717 Award (APR9/1017) of the Academy of Medical Sciences awarded to C.G. O.C. is an Einstein
718 Independent Researcher (ESR-2023-770) funded by the Einstein Foundation Berlin. Additionally,
719 this project was supported by funding to D.P. by award of the Jean Clayton Fund 2025, Liverpool
720 School of Tropical Medicine, and the Rosetrees Seedcorn Award 2025 for the project “Targeting
721 HIV Accessory Proteins Toward Therapeutic Intervention and Cure (TAcTIC)”.
722
723
724

Figure 1 Postmus *et al*., 2026

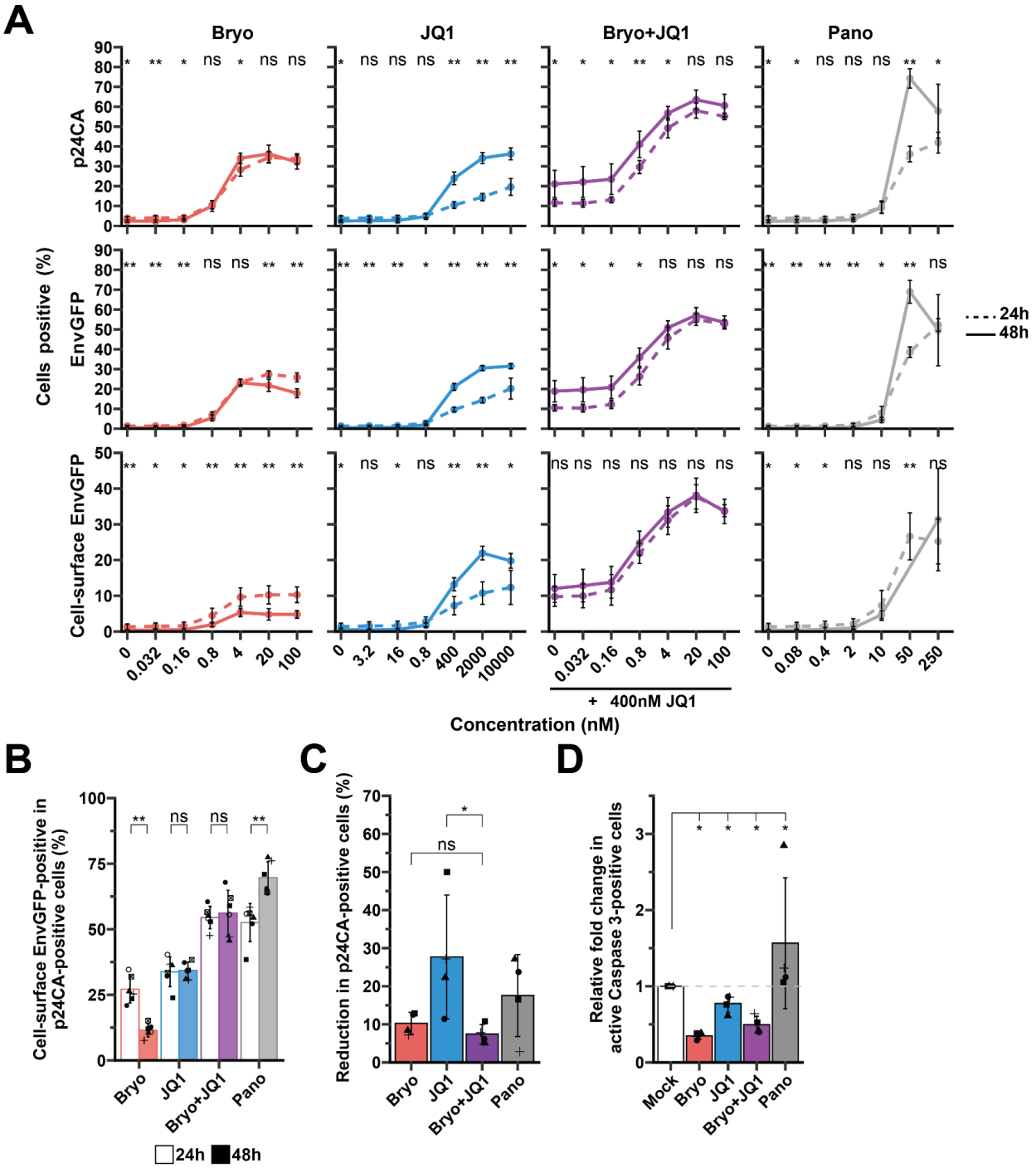

725

726

727 **Figure 1. Bryostatin-1, despite its latency reversal activity, imposes a restriction to HIV-1**

728 **Env cell-surface presentation**

729

730 A) Titration of bryostatin-1, JQ1, bryostatin-1 in the presence of 400nM JQ1, and
731 panobinostat on JLEG.1 cells, measuring intracellular p24CA, total EnvGFP and cell-
732 surface levels of EnvGFP at 24h and 48h post-reactivation by flow cytometry; n=6,
733 Wilcoxon rank-signed test.

734 B) Quantification of cell-surface EnvGFP-positive cells within the p24CA-positive population
735 in JLEG.1 cells treated for 24h and 48h with bryostatin-1 (4nM), JQ1 (400nM), a
736 combination of bryostatin-1 and JQ1, or panobinostat (50nM), measured by flow
737 cytometry; n=6 , Wilcoxon rank-signed test.

738 C) Reduction in p24CA-positive cells for JLEG.1 T-cells treated with the indicated LRAs for
739 24h, followed by co-culture with PBMCs from HIV-negative donors in the presence of sera
740 from PLWH for 4h to induce antibody-dependent cytotoxic killing; n=4 PBMC donors, t-
741 test on log-normalised data.

742 D) Relative proportion of JLEG.1 T-cells expressing cleaved, active Caspase 3 upon
743 indicated treatments for 24h, followed by exposure to etoposide (16h) to induce intrinsic
744 apoptosis, measured by flow cytometry. Expression was normalised to the mock condition;
745 n=4, Wilcoxon rank-signed test.

746 *** $p < 0.001$; ** $p < 0.01$; * $p < 0.05$. Indicated is the arithmetic mean ± SD.

747

Figure 2 Postmus *et al.*, 2026

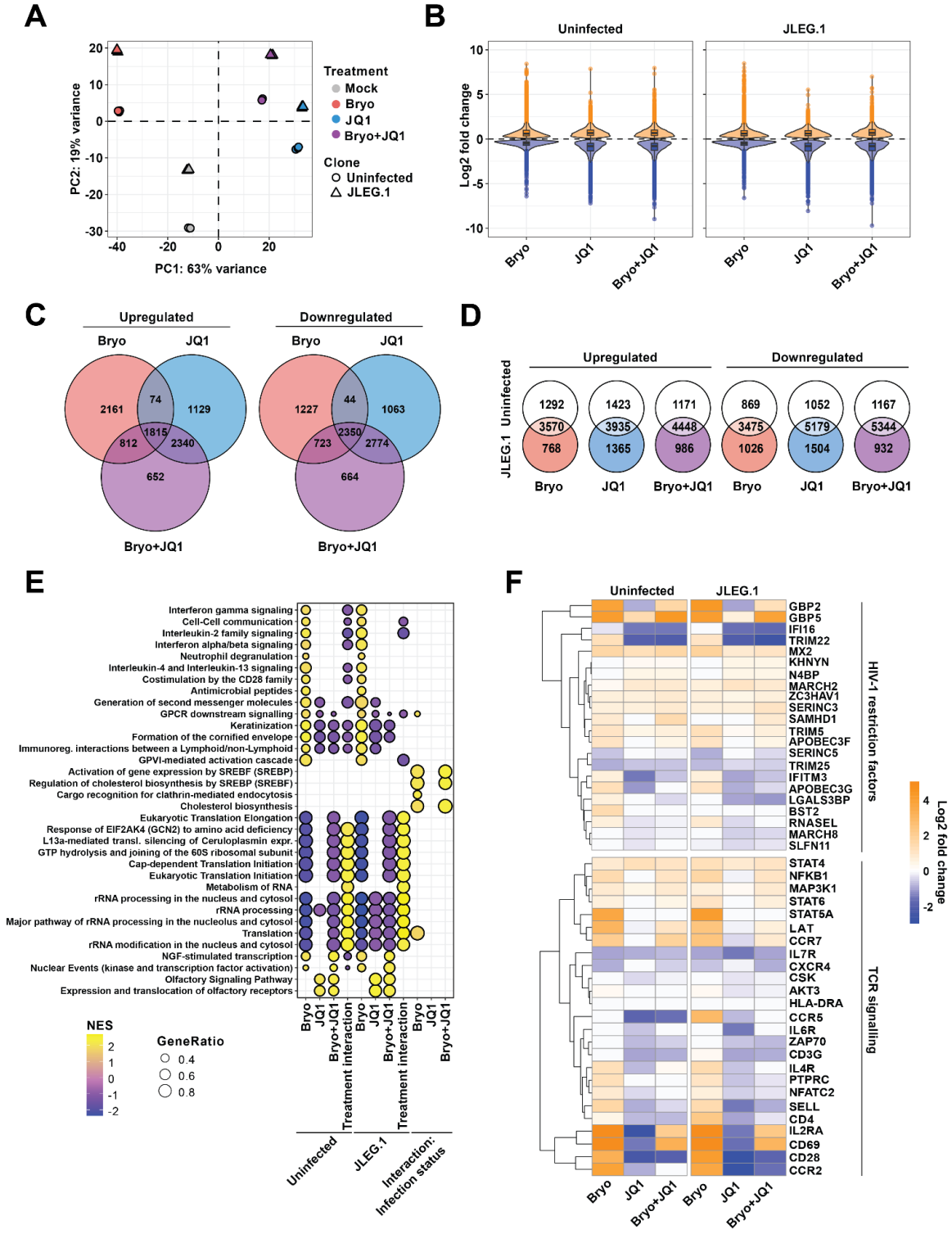

Figure 2. Bryostatin-1 treatment induces expression of T-cell activation markers and GBPs.

751 A) Principal component analysis (PCA) plot of the transcriptomes of the JLEG.1 clone, as
752 well as of an uninfected clone of same origin, after indicated treatments for 24h; n=3 for
753 each clone and treatment combination.
754 B) Violin plots indicating the statistically significantly up- (orange) and downregulated (blue)
755 genes in the indicated treatments, relative to the mock condition ($p_{adjusted} < 0.05$).
756 C) Venn diagrams illustrating the overlap in statistically significantly differentially up- and
757 downregulated genes relative to the mock condition in JLEG.1 cells between treatments
758 ($p_{adjusted} < 0.05$).
759 D) Venn diagrams illustrating the overlap in statistically significantly differentially up- and
760 downregulated genes relative to the mock condition for the indicated treatments between
761 the uninfected clone (top) and JLEG.1 cells (bottom) ($p_{adjusted} < 0.05$).
762 E) Gene set enrichment analysis of differentially upregulated genes for each treatment
763 relative to the mock condition by respective cell line using the Gene Ontology: Biological
764 Pathway database. Indicated are the top 20 enriched pathways by treatment and cell line.
765 Indicated is also the interaction effect, representing the effect on the enrichment of certain
766 pathways that is modulated by the presence of a provirus.
767 F) Fold change in gene expression for each LRA treatment relative to the mock condition,
768 determined for the uninfected and JLEG.1 clone respectively, for selected genes
769 corresponding to known HIV-1 restriction factors and TCR signalling pathways.
770

Figure 3 Postmus *et al.*, 2026

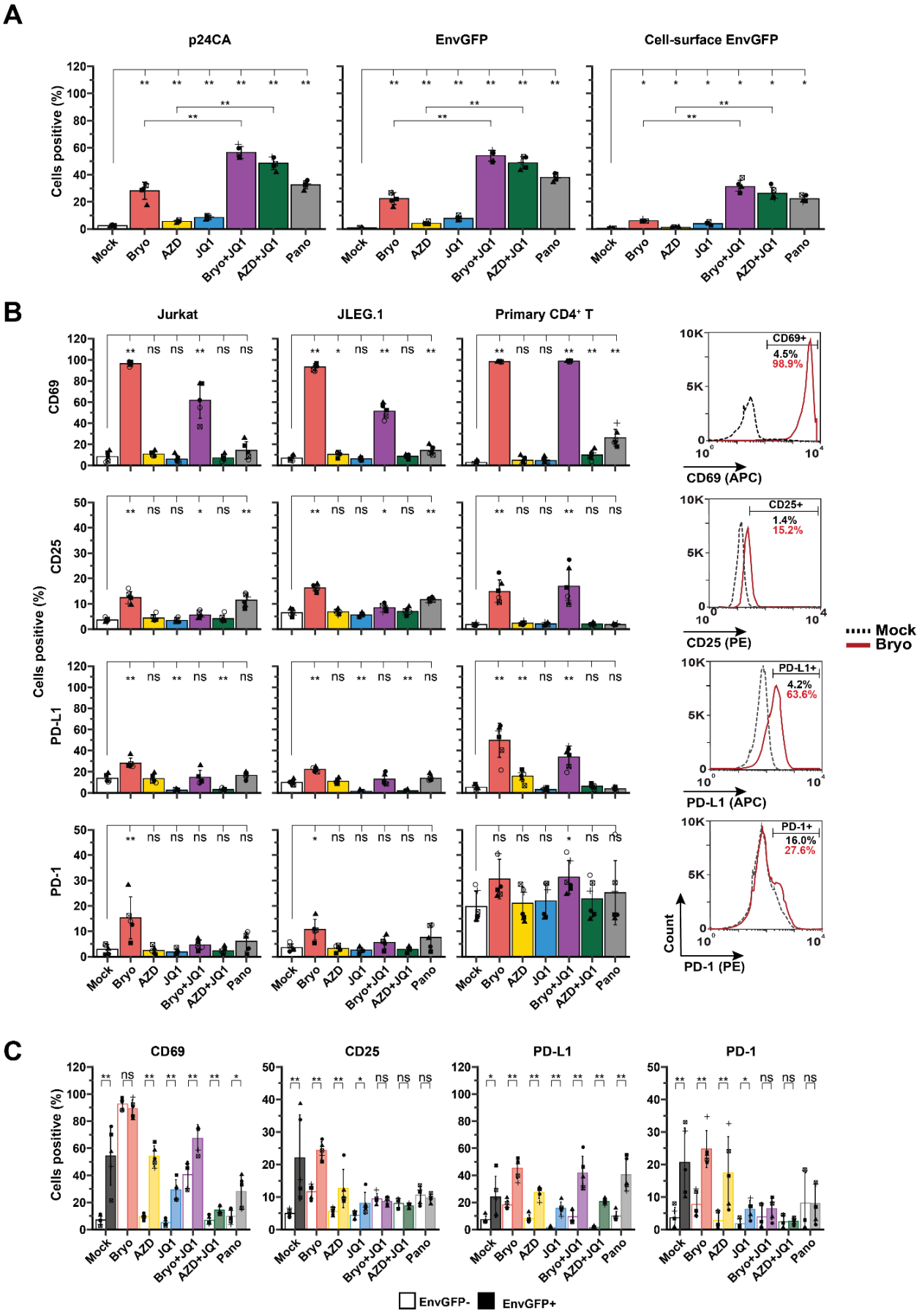

772 **Figure 3. Bryostatin-1 treatment and reactivation of proviral transcription, but not AZD5582**
773 **treatment, promote T-cell activation**

774 A) Percentage of cells expressing HIV-1 p24CA (left panel), total EnvGFP (middle panel) and
775 cell-surface EnvGFP (right panel) in JLEG.1 T-cells treated as indicated for 24h, quantified
776 by flow cytometry; n=5.

777 B) Percentage of cells positive for cell-surface expression of T-cell activation markers CD25,
778 CD69, PD-L1 and PD-1 in JLEG.1; uninfected Jurkat T-cells; and unstimulated, primary
779 $CD4^+$ T-cells from HIV-1-negative donors treated as indicated for 24h, quantified by flow
780 cytometry; n=6. Representative flow cytometry histograms for mock-treated and
781 bryostatin-1-treated primary $CD4^+$ T-cells are provided.

782 C) Expression of T-cell activation markers on JLEG.1 T-cells, treated as above, assessed for
783 EnvGFP-positive and EnvGFP-negative T-cells, respectively, in the same sample and
784 quantified by flow cytometry; n=6.

785 Wilcoxon rank-signed test. *** $p < 0.001$; ** $p < 0.01$; * $p < 0.05$. Indicated is the arithmetic mean
786 ± SD.

787

788

789

790

Figure 4 Postmus *et al.*, 2026

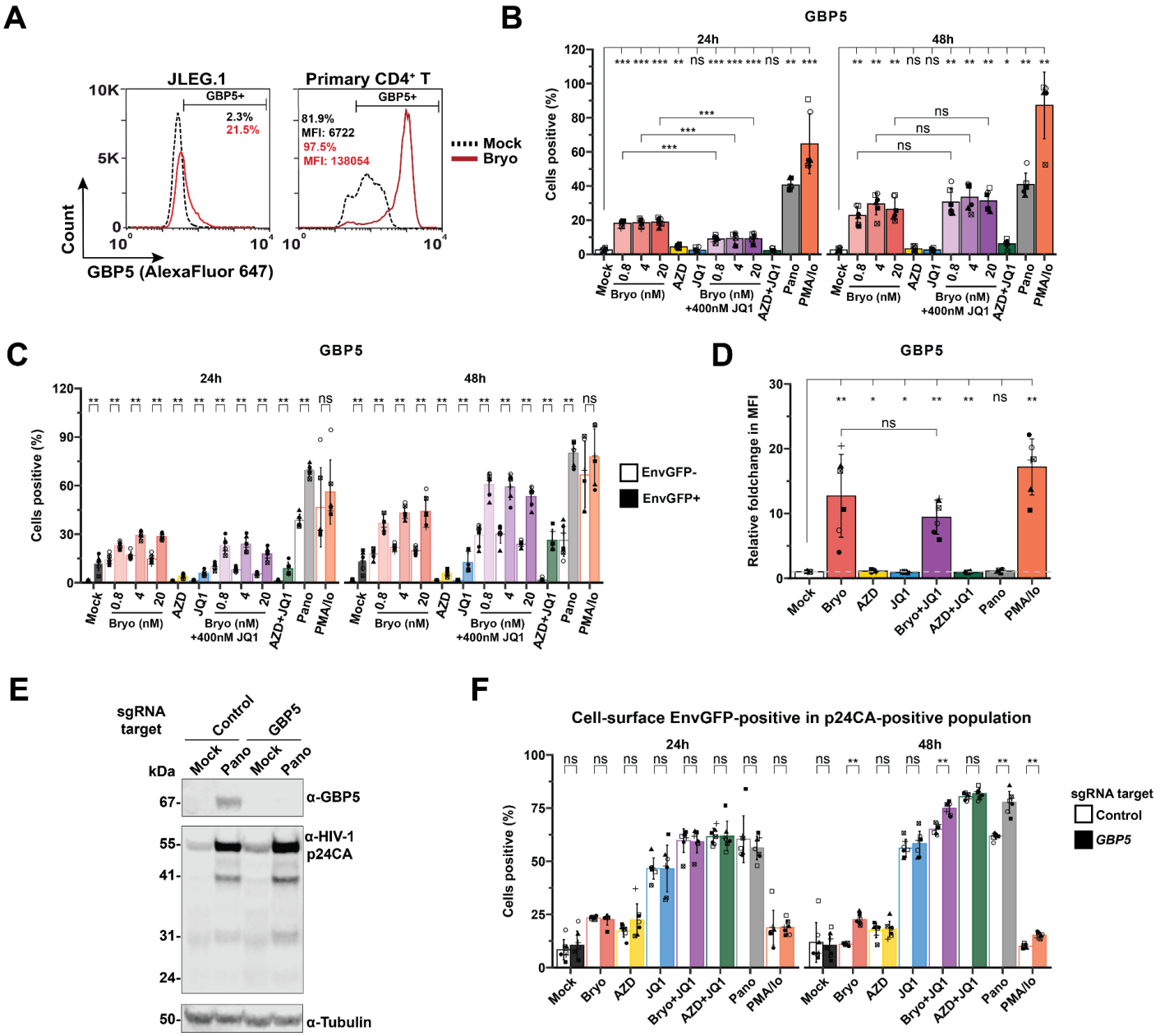

Figure 4. GBP5 expression, induced by bryostatin-1 treatment and the reactivating provirus, is accompanied by reduced cell-surface levels of EnvGFP

A) Representative flow cytometry histograms illustrating the increase in GBP5 expression, indicated by percentage of GBP5-positive cells or the mean fluorescence intensity (MFI)

796 of the GBP5 signal for JLEG.1 (left) and primary $CD4^+$ T-cells (right) after mock treatment
797 and bryostatin-1 treatment for 24h.
798 B) Percentage of GBP5-positive JLEG.1 T-cells after mock treatment or treatment with the
799 indicated LRAs, including varying, indicated concentrations of bryostatin-1, for 24h and
800 48h, respectively, quantified by flow cytometry; n=5-7.
801 C) Percentage GBP5-positive JLEG.1 T-cells, within EnvGFP-negative and EnvGFP-positive
802 cells of the same sample, treated as in A) for 24h and 48h; n=5-6.
803 D) Fold change of GBP5 MFI, relative to the mock-treated condition, for primary $CD4^+$ T-cells
804 treated with the indicated LRAs.
805 E) Representative immunoblot showing the CRISPR/Cas9-mediated knockout of the *GBP5*
806 gene in JLEG.1 T-cells, either mock-treated or treated with panobinostat as a known
807 inducer of GBP5 for 24h. The viral Gag proteins (detected by anti-p24CA antibody) are
808 included as a control for reactivation efficacy. Tubulin is included as a loading control..
809 F) Expression of cell-surface EnvGFP in the HIV-1 p24 capsid-positive population for *GBP5*
810 knockout or control JLEG.1 T-cells after mock treatment or treatment with the indicated
811 LRAs for 24h and 48h.
812 Wilcoxon rank-signed test. *** $p < 0.001$; ** $p < 0.01$; * $p < 0.05$. Indicated is the arithmetic
813 mean ± SD.
814

Figure 5 Postmus *et al.*, 2026

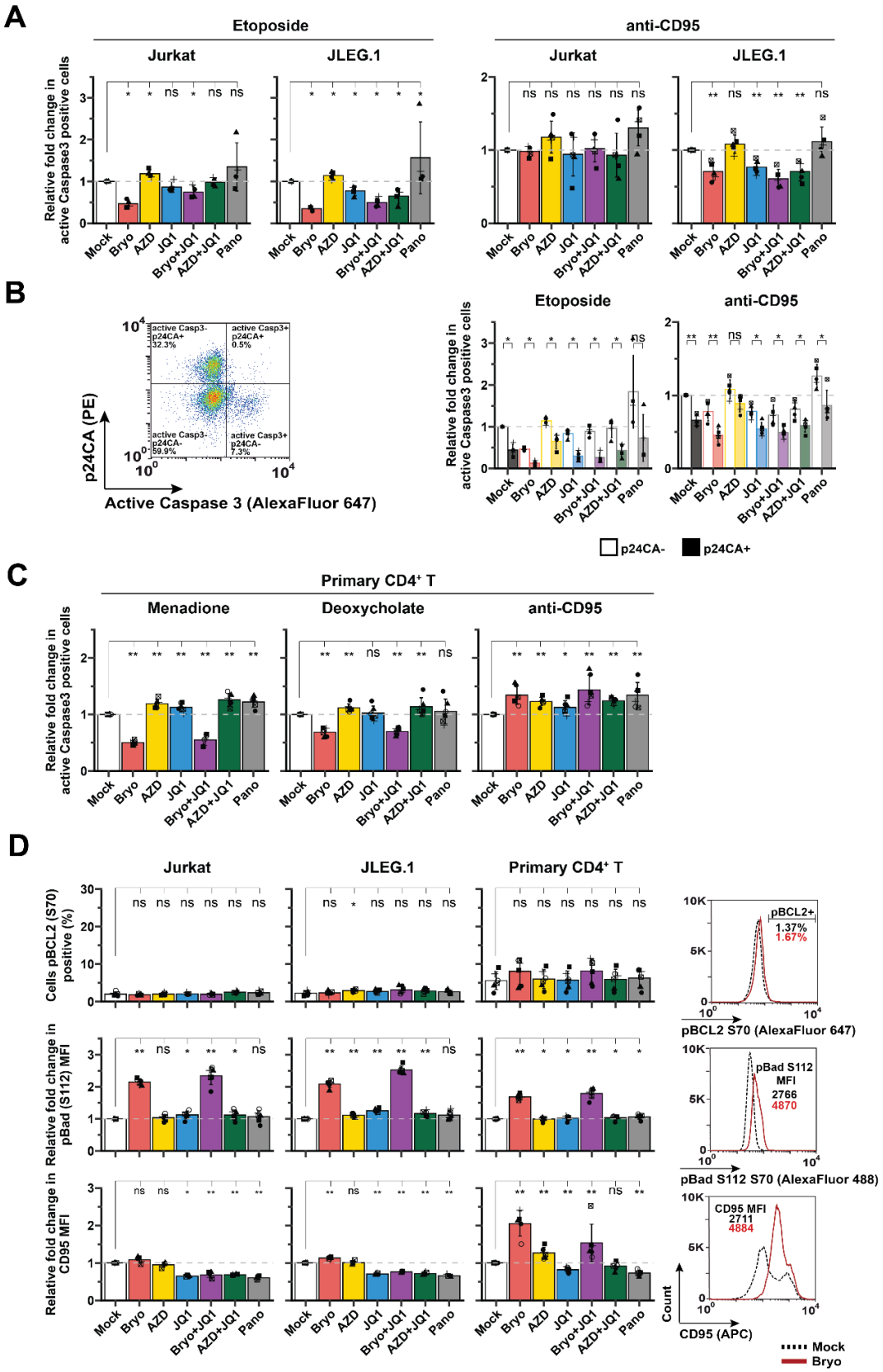

815

816

817 **Figure 5. Bryostatin-1 and the reactivating provirus both antagonise induction of apoptosis**

818

819 A) Relative expression of cleaved, active Caspase 3 as a marker of apoptosis in Jurkat and
820 JLEG.1 T-cells upon mock treatment or treatment with the indicated LRAs for 24h, followed
821 by exposure to either etoposide (16h, left) to induce intrinsic apoptosis or an activating,
822 anti-CD95 antibody in the presence of Protein G to induce extrinsic apoptosis (5h, right),
823 measured by flow cytometry. Expression was normalised to the mock condition; n=4-5.
824 B) Gating strategy used to determine the relative expression of active Caspase 3 in the p24
825 capsid-negative and p24 capsid-positive populations, respectively, within the same
826 sample (left) and the relative expression of active Caspase 3 in these populations for
827 JLEG.1 T-cells treated as in A) with the LRAs and apoptosis inducers indicated (right),
828 measured as in A); n=4-5.
829 C) Relative expression of active Caspase 3 in primary $CD4^+$ T-cells after mock treatment or
830 treatment with the indicated LRAs for 24h, then exposed for a further 24h to either
831 menadione or deoxycholate to induce intrinsic apoptosis, or an activating, anti-CD95
832 antibody in the presence of Protein G, measured as in A); n=6.
833 D) Expression of pBCL2 S70, pBad S112 after 1h of treatment or cell-surface CD95
834 expression after 24h of treatment in Jurkat, JLEG.1 and primary $CD4^+$ T-cells treated with
835 the indicated LRAs, measured by flow cytometry; n=6.
836 Wilcoxon rank-signed test. *** $p < 0.001$; ** $p < 0.01$; * $p < 0.05$. Indicated is the arithmetic
837 mean ± SD.

838

Figure 6 Postmus *et al.*, 2026

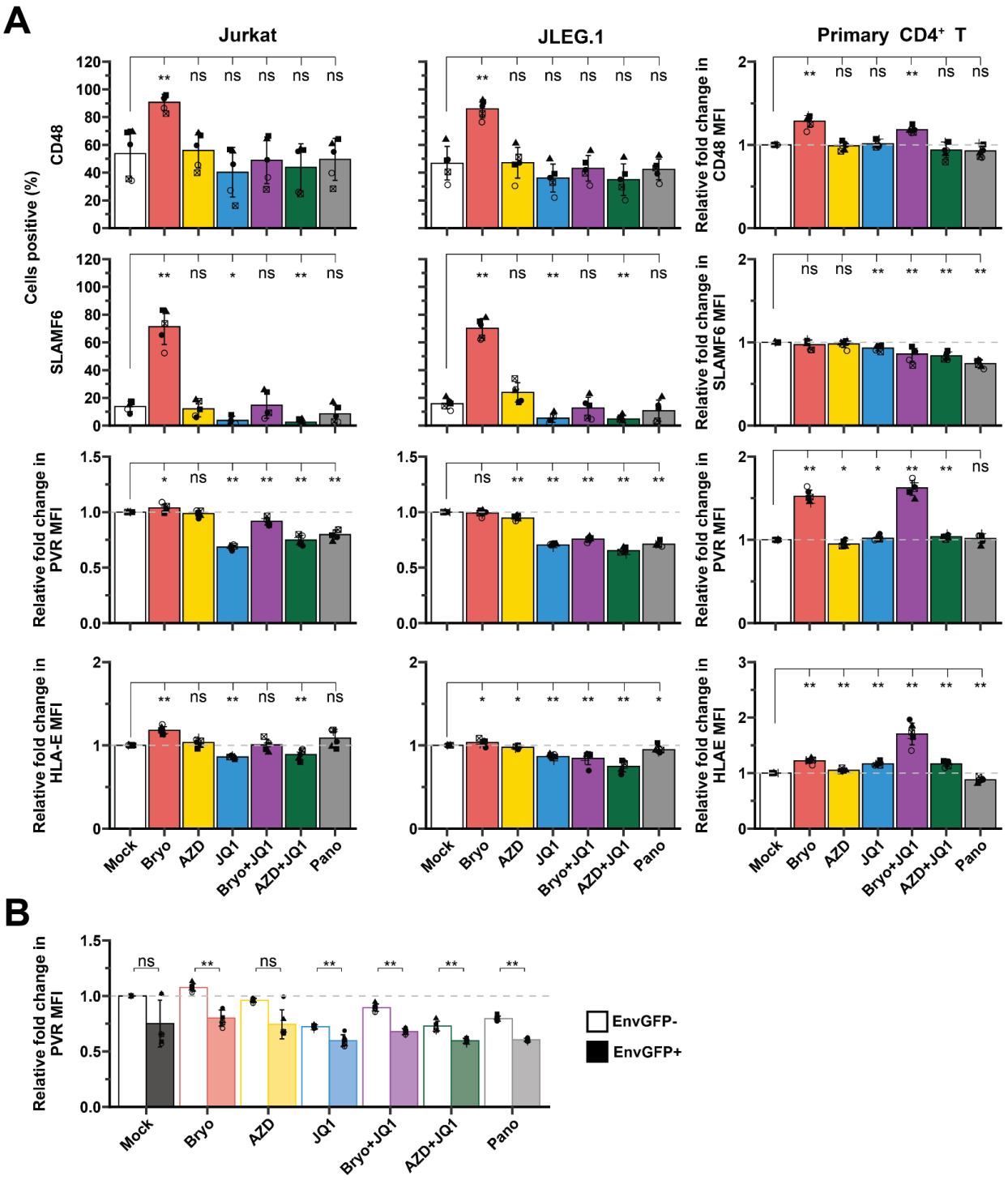

Figure 6. Blocks to ADCC after bryostatin-1 treated are unrelated to ADCC co-factor modulation

842 A) Cell-surface expression of ADCC co-factors CD48, SLAMF6 and and PVR, as well as the
843 inhibitory molecule HLA-E, in parental Jurkat, JLEG.1 and primary $CD4^+$ T-cells treated
844 with the indicated LRAs for 24h, measured by flow cytometry; n=6.
845 B) Relative expression of the NK cell ligand PVR in the EnvGFP- and EnvGFP+ populations
846 for JLEG.1 T-cells treated as in A), measured by flow cytometry. Expression was
847 normalised to the MFI of the EnvGFP- cells in the mock condition; n=6.
848 Wilcoxon rank-signed test. *** $p < 0.001$; ** $p < 0.01$; * $p < 0.05$. Indicated is the arithmetic
849 mean ± SD.
850

Figure 7 Postmus *et al.*, 2026

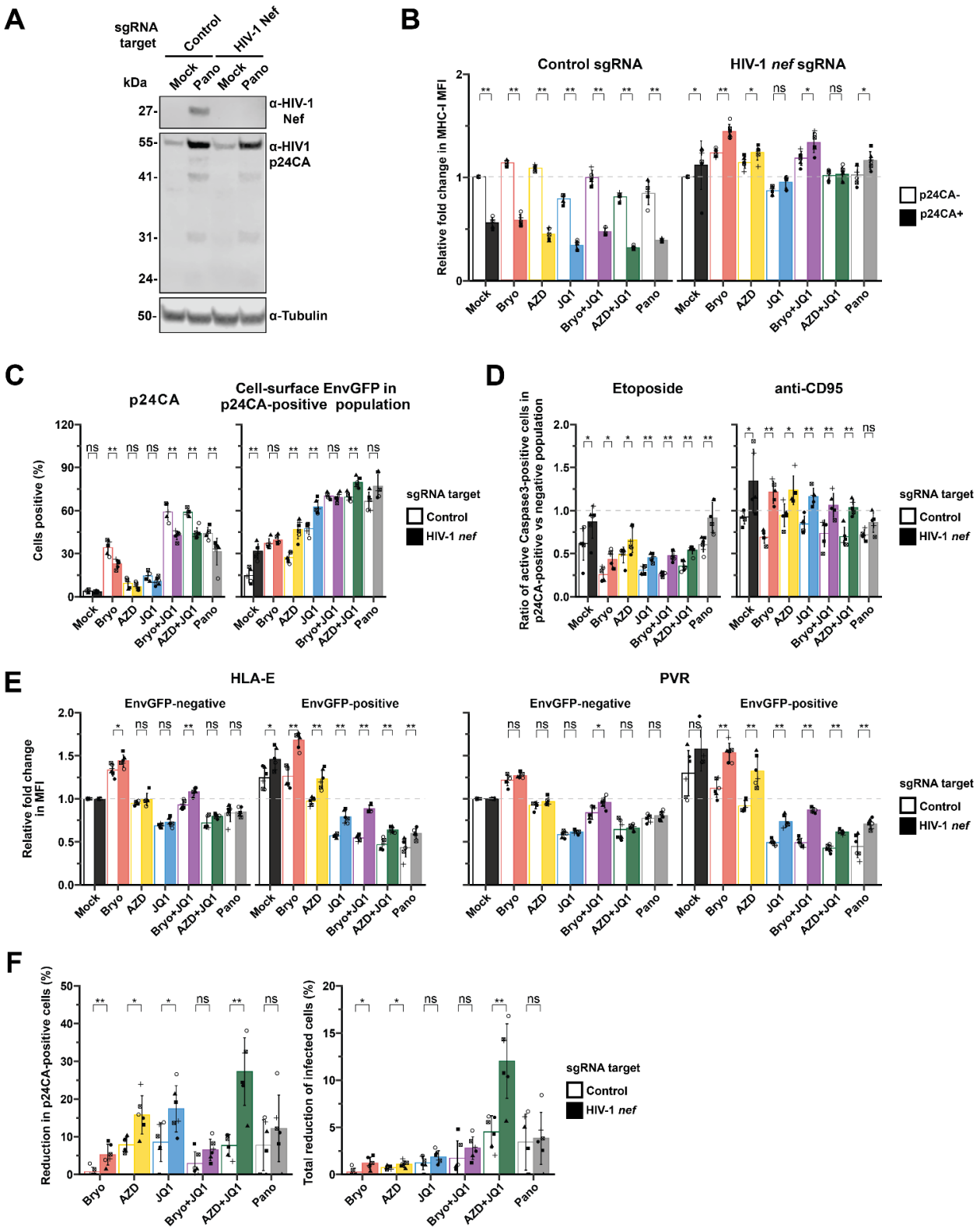

851

852 **Figure 7. Knockout of the viral *nef* gene increases susceptibility of HIV-1-reactivating T-**
853 **cells to apoptosis and ADCC-mediated killing**

854 A) Representative immunoblot showing the efficacy of the CRISPR/Cas9-mediated knockout
855 of the proviral *nef* gene in JLEG.1 T-cells, either mock-treated or treated with panobinostat
856 for 24h. The viral p55Gag protein is included as a control for treatment efficacy and Tubulin
857 is included as a loading control. Cells were lentivirally transduced with a vector encoding
858 Cas9 and an sgrRNA targeting *nef*, or a non-targeting, control sgRNA.

859 B) Relative fold change in the MFI of cell-surface MHC-I in *nef* knockout and control JLEG.1
860 T-cells for p24-negative and p24-positive T-cells in the same sample, respectively,
861 measured by flow cytometry. Expression was normalised to the MFI of the p24-negative
862 cells in the mock condition; n=6.

863 C) Expression of p24 and cell-surface EnvGFP in the p24CA-positive population of *nef*
864 knockout and control JLEG.1 T-cells, either mock-treated or treated with the indicated
865 LRAs for 24h, measured by flow cytometry; n=6.

866 D) Relative expression of cleaved, active Caspase 3 as a marker of apoptosis in *nef* knockout
867 and control JLEG.1 T-cells, mock-treated or treated for 24h with the indicated LRAs, then
868 exposed either to etoposide (16h, left) to induce intrinsic apoptosis or an activating, anti-
869 CD95 antibody in the presence of Protein G to induce extrinsic apoptosis (5h, right),
870 measured by flow cytometry. Expression was normalised to the mock condition; n=5-6.

871 E) Relative fold change in the MFI of cell-surface HLA-E (left) and PVR (right) in *nef* knockout
872 and control JLEG.1 T-cells for EnvGFP-negative and EnvGFP-positive cells in the same
873 sample. Expression was normalised to the MFI of the EnvGFP-negative cells in the mock
874 condition; n=6.

875 F) Reduction in p24CA-positive cells (left) and total reduction of infected cells for JLEG.1 T-
876 cells treated with the indicated LRAs for 24h, followed by co-culture with PBMCs from HIV-

877 negative donors in the presence of sera from PLWH for 4h to induce antibody-dependent
878 cytotoxic killing; n=6 PBMC donors.
879 Wilcoxon rank-signed test. *** $p < 0.001$; ** $p < 0.01$; * $p < 0.05$. Indicated is the arithmetic
880 mean ± SD.
881